Fırat Üniversitesi Deneysel ve Hesaplamalı Mühendislik Dergisi

# Parametrik Analiz ve Destek Vektör Makinesi Algoritması Kullanılarak İki Kademeli Kaskad Soğutma Sisteminin Termodinamik Performans Değerlendirmesi

Oğuzhan PEKTEZEL[1]*

[1]Makine Mühendisliği Bölümü, Mühendislik Fakültesi, Balıkesir Üniversitesi, Balıkesir, Türkiye.
[1]oguzhan.pektezel@balikesir.edu.tr

Geliş Tarihi: 24.04.2025
Kabul Tarihi: 7.06.2025

Düzeltme Tarihi: 24.05.2025

doi: https://doi.org/10.62520/fujece.1683037
Araştırma Makalesi

Alıntı: O. Pektezel, "Parametrik analiz ve destek vektör makinesi algoritması kullanılarak iki kademeli kaskad soğutma sisteminin termodinamik performans değerlendirmesi", Fırat Üni. Deny. ve Hes. Müh. Derg., vol. 4, no 2, pp. 406-423, Haziran 2025.

**Öz**

Bu çalışmada, ultra düşük sıcaklıklara ulaşabilen iki kademeli kaskad bir soğutma sisteminin termodinamik tasarımı yapılmış ve enerji ile ekserji analizleri gerçekleştirilmiştir. Dört soğutucu akışkan çiftinin—R744/R152a, R744/R32, R41/R152a ve R41/R32—performansı değerlendirilmiştir. -70 °C ile -50 °C arasındaki evaporatör sıcaklıkları ve 25 °C ile 45 °C arasındaki kondenser sıcaklıkları boyunca yürütülen parametrik analiz sonuçları, R41/R152a'nın en verimli çift olduğunu göstermiştir. -50 °C evaporatör sıcaklığında maksimum 1.421 COP değeri elde edilmiş ve en yüksek 0.4407 ekserji verimi -60 °C'de kaydedilmiştir. İkinci aşamada, COP ve ekserji verimini tahmin etmek için SVM yöntemi uygulanmış ve sırasıyla test setinde çok düşük MAE değerleri olan 0.0040 ve 0.0009 elde edilmiştir. Enerji-ekserji analizi ve SVM modellemesinin sonuçlarının, düşük sıcaklıklı kaskad soğutma sistemlerinin tasarımı için değerli bir rehberlik sağlaması beklenmektedir.

**Anahtar kelimeler:** Kaskad soğutma sistemi, R744, R41, R152a, R32, Destek vektör makinesi

*Yazışılan Yazar

İntihal Kontrol: Evet – Turnitin
Şikayet: fujece@firat.edu.tr

Firat University Journal of Experimental and Computational Engineering

FUJECE

# Thermodynamic Performance Evaluation of a Two-Stage Cascade Refrigeration System Using Parametric Analysis and Support Vector Machine Algorithm

Oğuzhan PEKTEZEL[1*]

[1]Department of Mechanical Engineering, Faculty of Engineering, Balıkesir University, Balıkesir, Türkiye.
[1]oguzhan.pektezel@balikesir.edu.tr

Received: 24.04.2025
Accepted: 7.06.2025

Revision: 24.05.2025

doi: https://doi.org/10.62520/fujece.1683037
Research Article

Citation: O. Pektezel, "Thermodynamic performance evaluation of a two-stage cascade refrigeration system using parametric analysis and support vector machine algorithm", Firat Univ. Jour.of Exper. and Comp. Eng., vol. 4, no 2, pp. 406-423, June 2025.

**Abstract**

In this study, a thermodynamic design of a two-stage cascade refrigeration system capable of reaching ultra-low temperatures was developed, and energy and exergy analyses were conducted. The performance of four refrigerant pairs—R744/R152a, R744/R32, R41/R152a, and R41/R32—was evaluated. Parametric analysis results, carried out across evaporator temperatures ranging from -70 °C to -50 °C and condenser temperatures between 25 °C and 45 °C, showed that R41/R152a was the most efficient pair. A maximum COP of 1.421 was achieved at -50 °C evaporator temperature, and the highest exergy efficiency of 0.4407 was recorded at -60 °C. In the second phase, an SVM approach was applied to predict COP and exergy efficiency, yielding very low MAE values of 0.0040 and 0.0009 in the test set, respectively. The outcomes of the energy-exergy analysis and SVM modeling are expected to provide valuable guidance for designing low-temperature cascade refrigeration systems.

**Keywords:** Cascade refrigeration system, R744, R41, R152a, R32, Support vector machine

*Corresponding author

## 1. Introduction

According to ASHRAE, equipment capable of reaching temperatures below −50 °C—as referenced in Directive (EU) No 517/2014—is categorized as ultralow-temperature (ULT) refrigeration, encompassing evaporating temperatures as low as −100 °C [1]. The recent emergence of Sars-CoV-2 vaccines has brought attention to a long-standing issue in society, namely deep freezing, as the Pfizer-BioNTech vaccine needs to be stored at temperatures between –60 °C and –80 °C [2]. In recent years, the demand for ultra-low temperature freezers capable of reaching −80 °C has grown substantially in various industrial fields, including medical storage, food preservation, electronic data processing, and chemical manufacturing [3].

Research has indicated that the primary sources of energy consumption and environmental pollution are associated with power generation, heating, and cooling processes [4]. Refrigeration systems are significant energy consumers due to the substantial power required for compression processes. Considering widely used air-conditioning applications, such as air conditioners, it is well-established that refrigeration systems cause a notable portion of global energy consumption, with estimates suggesting that approximately 17% of the world's energy usage is attributed to refrigeration systems [5].

Although refrigeration systems that utilize waste heat and renewable energy offer notable advantages for a sustainable energy future, their coefficient of performance remains relatively low, limiting their widespread adoption in comparison to vapor compression systems [6]. A classical single-stage refrigeration configuration is inadequate for achieving low temperatures due to the excessive compression ratio and large suction volume required by the compressor [7]. Cascade designs are particularly efficient in areas requiring high-pressure ratios—such as commercial refrigeration for food freezing or high-temperature heat pumps—where, in multi-stage configurations, the refrigerant for each stage is chosen based on its NBP [8-10]. A CRS, which involves multistage refrigeration circuits, aims to optimize thermal efficiency by employing multiple cycles, where a cascade heat exchanger integrates two classical refrigeration cycles, each with a separate refrigerant, operating at different temperature levels [11].

Currently, enhancing the performance of CRS and selecting appropriate refrigerants have become prominent research topics, with numerous studies focusing on analyzing and optimizing CRS performance using various refrigerant alternatives. Sun, Liang, Liu, Ji, Zang, Liang and Guo [12] investigated the thermal performance of cascade refrigeration systems using R41/R404A and R23/R404A refrigerants. Their study revealed that the R41/R404A system outperformed the R23/R404A system in terms of both lower input power and higher COP. The maximum exergy efficiency achieved by R41/R404A was 44.38%, while R23/R404A reached 42.98%. The results suggest that R41 is a more promising alternative to R23 in cascade refrigeration systems. Ye, Yan, Zhou and Yang [13] performed a thermodynamic analysis to enhance the design and operational parameters of an ultra-low temperature CRS by applying an ANN method. Their study identified that the condensing temperature of the low-temperature cycle achieves an optimal point, maximizing the system's coefficient of performance and exergy efficiency, while simultaneously minimizing compressor power consumption and exergy destruction. The ANN model demonstrated good predictive accuracy, with an MAE of 0.0027 for COP, 0.9090 for compressor power, 1.0314 for exergy destruction, and 0.1691 for exergy efficiency. Chen, Yang, Shi, Chen, Chi, Liu, Zhao and Li [14] conducted a study to design a cascade refrigeration system capable of achieving ultra-low temperatures from -80°C to -50°C. They replaced the high-temperature cycle gas R404A with natural refrigerant $NH_3$ and used R1150, R170, and R41 as environmentally friendly alternatives to replace the low-temperature cycle fluid R23. The study examined the effects of internal heat exchangers and two-stage compression on system performance. The results showed that the optimal COP of the $NH_3$/R1150, R170, and R41 systems was 15.79%, 18.58%, and 16.17% higher than that of the R404A/R23 system, with $NH_3$/R170 demonstrating the best performance. Faruque, Uddin, Salehin and Ehsan [11] conducted a comprehensive study on the thermodynamic performance of a two-stage cascade refrigeration system using hydrocarbon refrigerants. They selected refrigerants based on characteristics like molecular weight, freezing point, and global warming potential, using Trans-2-butane for the lower-temperature circuit and Toluene, Cyclopentane, and Cis-2-butane for the higher-temperature circuit. Their findings indicated that the highest COP and exergy efficiency were achieved with Trans-2-butane in the lower temperature circuit and Toluene in the higher temperature circuit. Furthermore, the use of hydrocarbon refrigerants led to a 7.21% improvement in COP compared to previously employed refrigerants. Ji, Liu, Pan and Li [15] conducted a study on the comprehensive performance of an ultra-low temperature cascade refrigeration arrangement, focusing on energy, exergy, environmental, and exergoeconomic factors. They compared eight environmentally friendly refrigerant pairs, including R1270-R1150, R1234yf-R1150, R290-R1150, R1234yf-R170, R717-R1150, R290-R170, R1270-R170, R717-R170 to evaluate the refrigeration performance. The study found that the R290-R170 pair performed optimally, enhancing COP by 5.94%, reducing power consumption by 5.68%, cutting $CO_2$ emissions by 29.67%, and lowering exergy economic cost by 5% compared to the R404A-R508B pair.

The literature review reveals that most studies on cascade refrigeration systems focus solely on thermodynamic analysis using various refrigerant combinations, while applications involving artificial intelligence in these systems remain quite limited. The novelty of this study lies in the implementation of the SVM method to a cascade refrigeration system to predict COP and exergy efficiency. Another original aspect of the research is the investigation of energy and exergy performance of R152a and R32—refrigerants whose performance in high-temperature cycles has been scarcely examined—when combined with R744 and R41 used in the low-temperature cycle. An SVM approach and the results achieved in this research are expected to greatly aid in optimizing the design and predicting the performance of cascade refrigeration systems with two-stage configuration, while also providing a solid foundation for future experimental validations.

## 1.1. Utilized refrigerants

Carbon dioxide, classified as a natural refrigerant with the ASHRAE designation R744, has long been utilized in refrigeration applications due to its negligible ODP and exceptionally low GWP [16]. R744 has been employed in a wide range of vapor compression systems for more than 130 years [17]. It is denser than air, exhibits no toxicity or flammability, is widely present in the atmosphere, is frequently generated as a byproduct in numerous industrial processes, and is a cost-effective refrigerant characterized by its low liquid density, which contributes to reduced system dimensions and a smaller refrigerant charge requirement [18].

R41, a non-toxic and environmentally favorable refrigerant with thermophysical properties similar to R23 and a considerably lower global warming potential, has gained attention as a low-temperature cycle fluid in cascade systems, and although its flammability presents a limitation, ongoing developments in refrigerant blends are anticipated to enable its practical use soon [12]. R41 and R744 exhibit comparable thermophysical characteristics, including nearly identical normal boiling points [19]. Despite its potential, the adoption of R744 as a future refrigerant is hindered by its high operating pressure, whereas alternatives such as R170, R1150, and R41 have been proposed to replace R23 and R508B in ultra-low temperature refrigeration systems [20].

Among the alternatives to R410A, R32 has been one of the most extensively investigated refrigerants, showing notable enhancements in both cooling capacity and coefficient of performance; however, its primary drawback lies in the elevated discharge temperatures it produces relative to R410A [21]. R-410A, the refrigerant that R-32 is designed to substitute, is composed of 50% R-32 and 50% R-125—the latter also widely utilized as a fire suppressant—and similarly, most of the newly developed low-GWP blends incorporate R-32 in their formulation [22]. Due to its pure substance nature, R32 exhibits no temperature glide [23].

Initially excluded from refrigeration applications due to its flammability, R-152a—now reconsidered following regulatory concerns over high-GWP hydrofluorocarbons under the F-Gas Regulation and Kigali Amendment—is the only HFC listed in ASHRAE Standard 34 with a GWP below 150, exempting it from restrictions such as reduction, substitution, or prohibition [24]. R152a closely resembles R134a in terms of volumetric cooling capacity and operating pressures, yet demonstrates superior performance in energy efficiency, mass flow rate, and vapor density [25].

Table 1 shows properties of the refrigerants used in analyses [1].

**Table 1.** Properties of utilized refrigerants

| *Cycle* | *Refrigerant* | *ODP* | *$GWP_{100\text{-}yr}$ ($CO_2$-eq)* | *ASHRAE Safety Group* | *NBP (°C)* | *Molecular Weight (kg $mol^{-1}$)* | *Critical Temperature (°C)* | *Critical Pressure (MPa)* |
|---|---|---|---|---|---|---|---|---|
| LTC | R744 | 0 | 1 | A1 | -78.46 | 44.01 | 30.98 | 7.38 |
| LTC | R41 | 0 | 116 | A2 | -78.31 | 34.03 | 44.13 | 5.9 |
| HTC | R152a | 0 | 138 | A2 | -24.02 | 66.05 | 113.26 | 4.52 |
| HTC | R32 | 0 | 677 | A2L | -51.65 | 52.02 | 78.11 | 5.78 |

## 2. Materials and Methods

### 2.1. Two-stage cascade refrigeration system

The schematic flow diagram of a two-stage cascade refrigeration system is depicted with all system components in Figure 1. The system is primarily comprised of two compressors, one evaporator, one condenser, two expansion valves, and a cascade heat exchanger. The low and high-temperature cycles operate with two different refrigerants. In refrigeration systems employing a cascade cycle, achieving the desired low chamber temperatures requires the refrigerant passing through the evaporator to be at extremely low temperatures. In the low-temperature cycle, the compressor increases the pressure and temperature of the refrigerant and directs it to the cascade heat exchanger. The cascade heat exchanger has two roles: it functions as a condenser for the low-temperature circuit and as an evaporator for the high-temperature circuit. Afterward, the refrigerant is sent to the expansion valve, where its pressure and temperature drop before it enters the evaporator. In the high-temperature (upper) cycle, the heat rejected by the low-temperature (lower) cycle is absorbed by the refrigerant in the upper cycle through the cascade heat exchanger. The pressure and temperature of the refrigerant in the high-temperature cycle are increased by the corresponding compressor. The refrigerant is then directed to the condenser, where it releases heat to the external environment. Finally, the refrigerant passes through the expansion valve, where its pressure and temperature are decreased before re-entering the cascade heat exchanger, thereby completing the cycle.

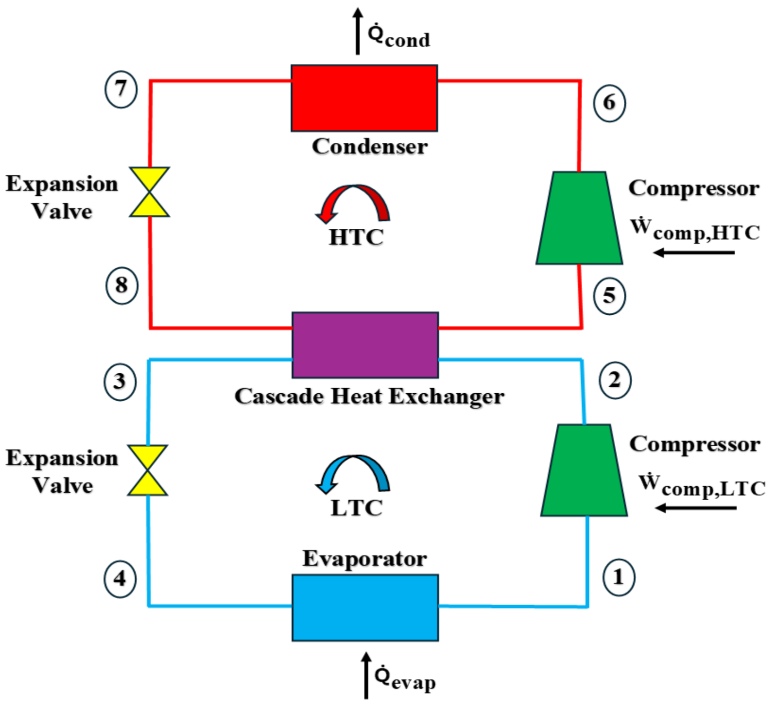


**Figure 1.** Schematic flow diagram of two-stage cascade refrigeration system

Thermodynamic design and thermal analyses of a two-stage cascade refrigeration system was carried out in EES software [26]. It is necessary to make some assumptions to model the system. All components within the system are considered to operate under steady-state conditions. Pressure losses and thermal exchanges throughout the entire piping system are disregarded. Variations in kinetic and potential energy throughout the system components are assumed to be negligible. The electrical power consumption of the fans associated with the condenser and evaporator is excluded from the analysis. Compression and expansion processes occurring in compressors and expansion valves are treated as adiabatic. No subcooling is present at the condenser outlets; in other words, the refrigerant quality at states 3 and 7 is assumed to be zero. Superheating at the evaporator exits is not considered; hence, the refrigerant quality at states 1 and 5 is taken as one. A temperature difference of 5 °C is maintained between the evaporator temperature and the refrigerated chamber temperature. Heat sink temperature of the condenser is accepted to be identical to the ambient temperature. Also, ambient temperature and pressure are taken as 25 °C and 101.325 kPa, respectively. Air is considered the external heat exchange fluid interacting with the refrigerant in both the condenser and the evaporator.

COP of the system can be calculated using Equation 1.

$$COP=\frac{\dot{Q}_{evap}}{\dot{W}_{comp,total}} \tag{1}$$

Total compressor power consumption can be detected with the following equation.

$$\dot{W}_{comp,total}=\dot{W}_{comp,LTC}+\dot{W}_{comp,HTC} \tag{2}$$

Cooling capacity is defined with Equation 3.

$$\dot{Q}_{evap}=\dot{m}_{LTC}(h_1-h_4) \tag{3}$$

Exergy of all points in the system can be calculated with Equation 4.

$$e_i=(h_i-h_0)-T_0(s_i-s_0) \tag{4}$$

Flow exergy is determined with multiplication of exergy and mass flow rate.

$$\dot{E}_i=\dot{m}_i e_i \tag{5}$$

Total exergy destruction of cascade refrigeration system is determined with the Equation 6.

$$\begin{aligned}\dot{E}_{dest,total}=&\dot{E}_{dest,evap}+\dot{E}_{dest,comp,LTC}+\dot{E}_{dest,CHX}+\dot{E}_{dest,valve,LTC}+\\&\dot{E}_{dest,comp,HTC}+\dot{E}_{dest,cond}+\dot{E}_{dest,valve,HTC}\end{aligned} \tag{6}$$

Exergy efficiency can be determined with Equation 7.

$$\eta_{ex}=1-\left(\frac{\dot{E}_{dest,total}}{\dot{W}_{comp,total}}\right) \tag{7}$$

Table 2 shows the design parameters required to model the system. The primary consideration in selecting the design parameters of the cascade refrigeration system, as presented in Table 2, was ensuring that the chosen analysis parameters are consistent with those used in similar studies in the literature. A cooling capacity of 10 kW has been commonly used as a design parameter in many cascade refrigeration studies in the literature [11, 12, 27]. Additionally, the selected evaporator temperatures are similar to the range applied in studies on two-stage cascade refrigeration systems in the literature [14, 28].

**Table 2.** Design parameters of the model

| *Operational Parameter* | *Input Value* | *Interval* |
|---|---|---|
| $\dot{Q}_{evap}$ | 10 kW | - |
| $\Delta T_{CHX}$ | 5 °C | - |
| $T_{evap}$ | -60 °C | -70 °C to -50 °C |
| $T_{cond}$ | 35 °C | 25°C to 45 °C |

## 2.2. SVM approach

Developed by Vapnik, the SVM is a classification algorithm renowned for its strong generalization capability, grounded in the structural risk minimization concept of statistical learning theory [29]. SVM is classified in the group of supervised machine learning approaches [30, 31]. In contrast to conventional neural network approaches, SVMs are capable of identifying a unique optimal solution, capturing nonlinear relationships effectively, and do not encounter dimensionality issues [32]. SVMs represent a robust and widely adopted approach in engineering, capable of handling complex problems with high efficiency [33]. Initially developed for constructing hyperplane-based decision boundaries, SVMs were later extended to handle nonlinear classification tasks through the use of the kernel trick [34]. The SVM algorithm starts by functioning within a space of lower dimensionality. Subsequently, the input data is transformed into a higher-dimensional feature space through the application of a kernel function. In this transformed space, the optimal separating hyperplane is then constructed. The SVM algorithm seeks to construct the most appropriate decision boundary, known as a hyperplane, that divides an n-dimensional space into definite classes, thereby making easier the accurate classification of new data points [35]. Support vectors refer to the data points that lie nearest to the decision boundary, while the margin denotes the distance between these points and the decision boundary itself [36].

For the optimization of the SVM, four different kernel functions were employed: normalized polynomial kernel, polynomial kernel, Pearson VII (PUK) kernel, and radial basis function kernel. Table 3 and Table 4 present the prediction errors for COP and exergy efficiency, respectively, obtained using the models built with these kernels. Upon examining the error values, it is evident that the Pearson VII (PUK) kernel function, represented in Model 3, resulted in the lowest prediction errors for both COP and exergy efficiency. Therefore, Model 3 was identified as the optimal model, and the Pearson VII (PUK) kernel function was used in the prediction phase. In studies conducted on thermal systems using the SVM algorithm, it has been found—consistent with the observations in this study—that the Pearson VII (PUK) kernel function results in lower prediction errors compared to other kernel functions [32, 37, 38].

**Table 3.** SVM models for COP

| *No* | *Kernel Type* | *Training Set MAE & RMSE for COP* | *Test Set MAE & RMSE for COP* |
|---|---|---|---|
| 1 | Normalized Polynomial Kernel Function | 0.0541 & 0.0792 | 0.0700 & 0.0926 |
| 2 | Polynomial Kernel Function | 0.0172 & 0.0266 | 0.0267 & 0.0335 |
| 3 | Pearson VII (PUK) Kernel Function | 0.0015 & 0.0033 | 0.0040 & 0.0064 |
| 4 | Radial Basis Function Kernel Function | 0.0963 & 0.1213 | 0.1155 & 0.1431 |

**Table 4.** SVM models for exergy efficiency

| *No* | *Kernel Type* | *Training Set MAE & RMSE for Exergy Efficiency* | *Test Set MAE & RMSE for Exergy Efficiency* |
|---|---|---|---|
| 1 | Normalized Polynomial Kernel Function | 0.0249 & 0.0320 | 0.0284 & 0.0370 |
| 2 | Polynomial Kernel Function | 0.0032 & 0.0043 | 0.0046 & 0.0057 |
| 3 | Pearson VII (PUK) Kernel Function | 0.0003 & 0.0004 | 0.0009 & 0.0015 |
| 4 | Radial Basis Function Kernel Function | 0.0306 & 0.0364 | 0.0339 & 0.0381 |

The formulation for a Pearson VII (PUK) kernel function is presented in equation 8. Here, $x_i$ and $x_j$ are used to express the vector arguments, σ is utilized to direct Pearson half-width, and a w term shows the tailing element of the peak.

$$K(x_i,x_j)=\frac{1}{\left[1+\left(\frac{2\sqrt{\left\|x_i-x_j\right\|^2}\sqrt{2^{(1/w)}-1}}{\sigma}\right)^2\right]^w} \tag{8}$$

To reduce prediction error, the hyperparameters C and Sigma were systematically adjusted within defined intervals. In the first step, Sigma was kept at its default value while the C parameter was varied between 1 and 7. It was found that setting C to 3.5 yielded the lowest error on both the training and testing datasets, making C = 3.5 the optimal choice. In the next step, with C fixed at 3.5, Sigma was varied between 1 and 4. The analysis revealed that the minimum error occurred when Sigma was set to 3, indicating that Sigma = 3 is the optimal setting.

## 3. Results

### 3.1. Parametric energy and exergy analysis results

Figure 2 shows the effect of evaporator temperature on COP. The increase in evaporator temperature from -70 °C to -50 °C led to a notable increase in COP across all working fluid pairs. A similar trend was observed in previous studies [12]. In the study conducted by Sun, Liang, Liu, Ji, Zang, Liang and Guo [12], when a 20°C increase in evaporator temperature was applied (from −60°C to −40°C) using the R41/R404A pair, the COP increased from approximately 1.05 to 1.5, corresponding to a 42.9% improvement. Similarly, in the present study, a comparable increase in COP was observed for a 20°C rise in evaporator temperature. For R41/R152a, the COP rose from 1 to 1.421, marking a 42.1% increase. R744/R152a exhibited a COP rise from 0.9769 to 1.408, equivalent to a 44.13% improvement. COP of R744/R32 couple increased from 0.9611 to 1.38 which indicated a 43.59% rise. In addition, a COP of R41/R32 improved by 41.62%, from 0.9836 to 1.393. At -50 °C, all refrigerant couples exhibited the highest COP. Overall, R41/R152a provides the highest COP values, making it the most efficient in terms of energy performance under varying evaporator temperatures.

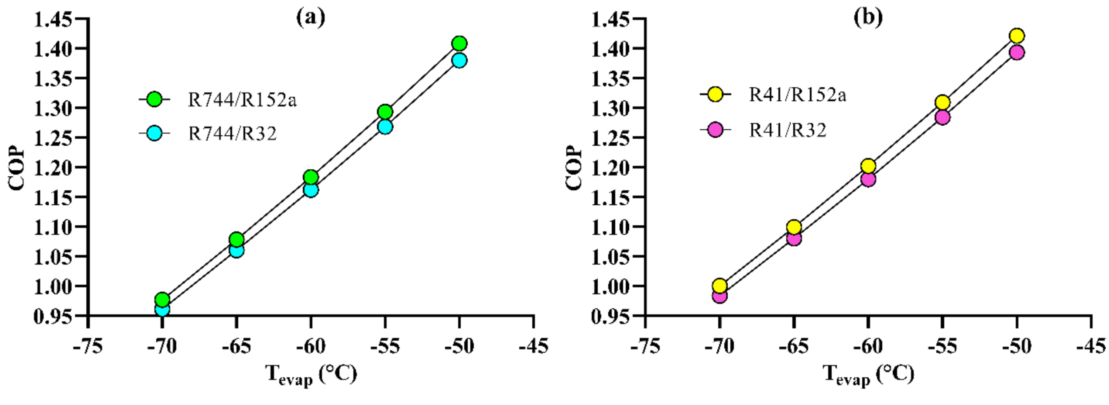


**Figure 2.** Evaporator temperature and COP relation

Figure 3 presents the influence of evaporation temperature on exergy efficiency. It can be stated that the exergy efficiency initially exhibits an increasing trend with the rising evaporator temperature; however, after reaching a peak point, it subsequently begins to decline. Similar observations were made in previous studies [28]. In the study conducted by Sun, Wang, Xie, Liu, Su and Cui [28], when the R41/R32 refrigerant pair was used, the exergy efficiency was approximately 0.39 at an evaporator temperature of −70°C, reaching a peak value of around 0.42 at −50°C, after which it began to decline. A similar trend was also observed in the present study. For the R744/R152a refrigerant pair, the exergy efficiency is 0.4224 at -70 °C, increases to its peak value of 0.4345 at -55 °C, and subsequently decreases to 0.4319 at -50 °C. For the R744/R32 refrigerant pair, the exergy efficiency exhibits an increasing trend from -70 °C to -55 °C, after which it begins to decline, reaching a value of 0.4234 at -50 °C. For the R41/R152a refrigerant pair, the exergy efficiency shows an increasing trend from -70 °C to -60 °C, rising from 0.4324 to 0.4407; thereafter, it begins to decrease. For the R41/R32 refrigerant pair, the exergy efficiency is 0.4253 at -70 °C, reaches its peak value of 0.4328 at -60 °C, and finally decreases to 0.4273 at -50 °C. In general, R41/R152a stands out as the most exergy-efficient refrigerant pair under changing evaporator temperatures.

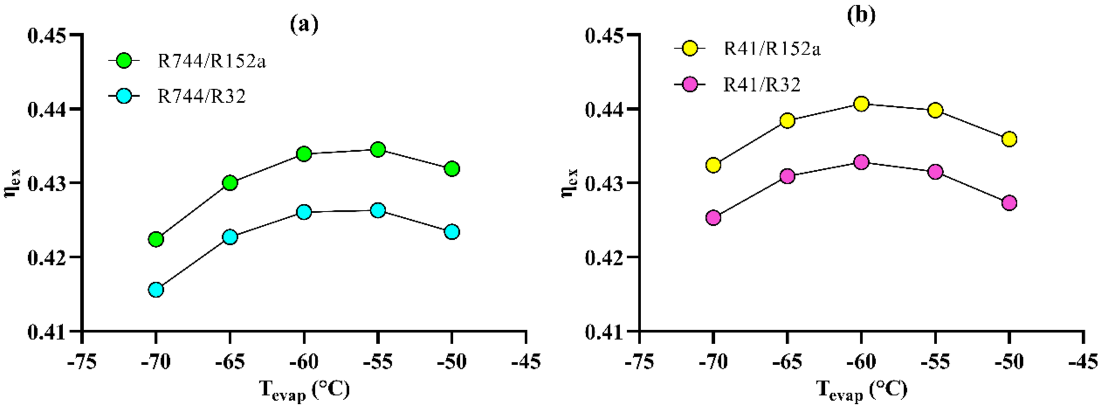


**Figure 3.** Evaporator temperature and exergy efficiency connection

Figure 4 depicts the impact of varying evaporator temperatures on total exergy destruction. Raising the evaporator temperature from -70 °C to -50 °C resulted in a decrease in total exergy destruction for all refrigerant couples. Previous studies revealed similar findings [11]. In the study conducted by Faruque, Uddin, Salehin and Ehsan [11], when the evaporator temperature was increased from −70°C to −50°C using the T2BUTENE/toluene refrigerant pair, the total exergy destruction decreased from approximately 4.75 kW to 3.38 kW, corresponding to a 28.8% reduction. Similarly, in the present study, a comparable reduction in total exergy destruction was observed when the evaporator temperature was varied within the same range. R41/R152a refrigerant couple showed a 30% reduction in total exergy destruction, from 5.676 kW to 3.971 kW. Total exergy destruction decreased by 29.6% for R41/R32, from 5.843 to 4.113 kW. In addition, a total exergy destruction of a R744/R152a pair dropped by 31.7%, from 5.912 to 4.036 kW. For R744/R32, total exergy destruction declined by 31.3%, from 6.081 to 4.178 kW. To sum up, R41/R152a exhibits the lowest total exergy destruction, making it the most thermodynamically favorable option in this respect.

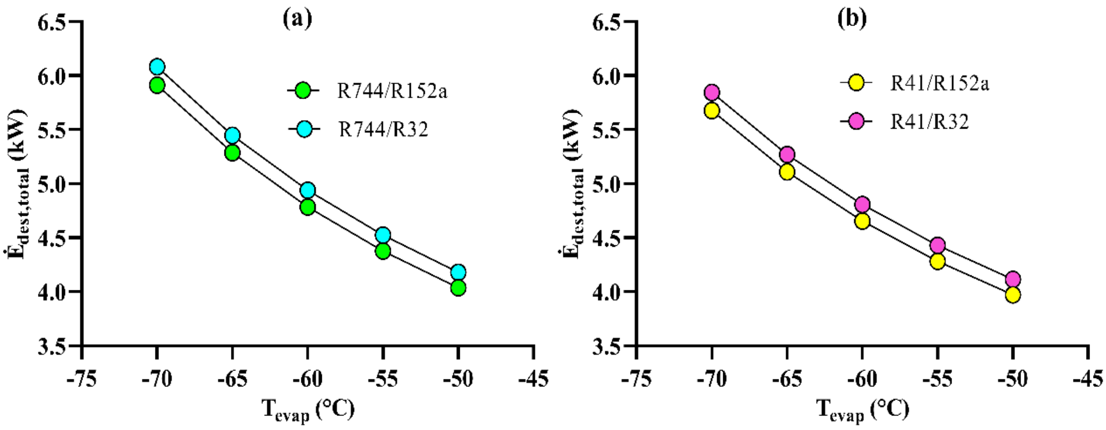


**Figure 4.** Evaporator temperature and total exergy destruction association

Figure 5 exhibits the influence of change in evaporator temperature on a total compressor power consumption of the system. As an evaporator temperature increased from -70 °C to -50 °C, total compressor power consumption decreased for all refrigerant couples. Previous studies demonstrated a similar behavior for compressor consumption [14]. A total compressor power consumption of a R41/R152a refrigerant pair declined from 10 to 7.039 kW, a 29.6% reduction. R41/R32 couple experienced a decrease in total compressor power consumption from 10.17 to 7.181 kW, a 29.4% drop. In addition, a total compressor consumption of R744/R152a dropped from 10.24 to 7.104 kW, representing a 30.6% reduction. For R744/R32, total compressor consumption fell by 30.3%, from 10.4 to 7.247 kW. Overall, R41/R152a demonstrates the lowest compressor power demand, indicating superior energy performance.

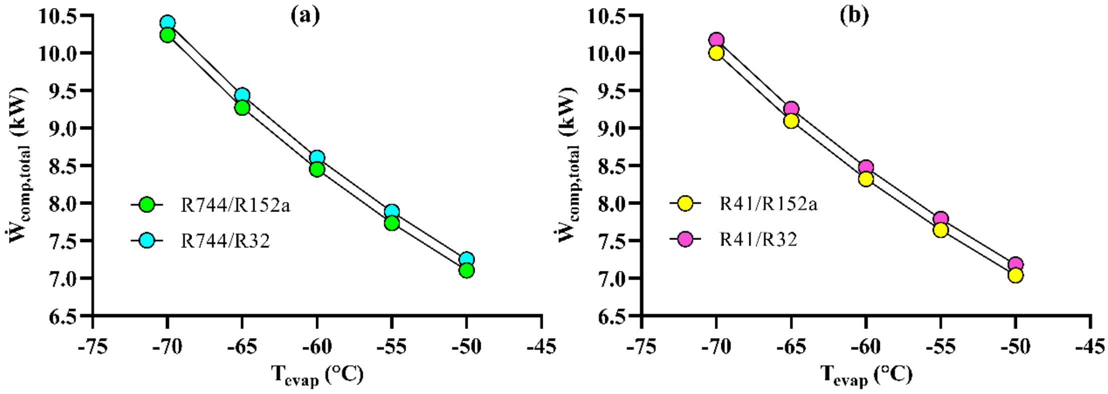


**Figure 5.** Change of total compressor consumption with evaporator temperature

Figure 6 illustrates the effect of condenser temperature on COP. Increasing condenser temperature from 25 °C to 45 °C caused a decline in COP for all refrigerant combinations. Similar findings regarding the decrease in COP values with increasing condenser temperature have also been reported in the literature [13]. COP of R41/R152a pair decreased from 1.445 to 0.9859, a 31.8% reduction. R41/R32 experienced a COP reduction of 31.5%, from 1.418 to 0.9709. COP of a R744/R32 refrigerant couple declined from 1.394 to 0.9574, a 31.3% decrease. In addition, increasing condenser temperature caused COP of R744/R152a to drop by 31.5%, from 1.42 to 0.9721. In general, R41/R152a delivers the highest COP under all condenser temperature levels, confirming its energy efficiency.

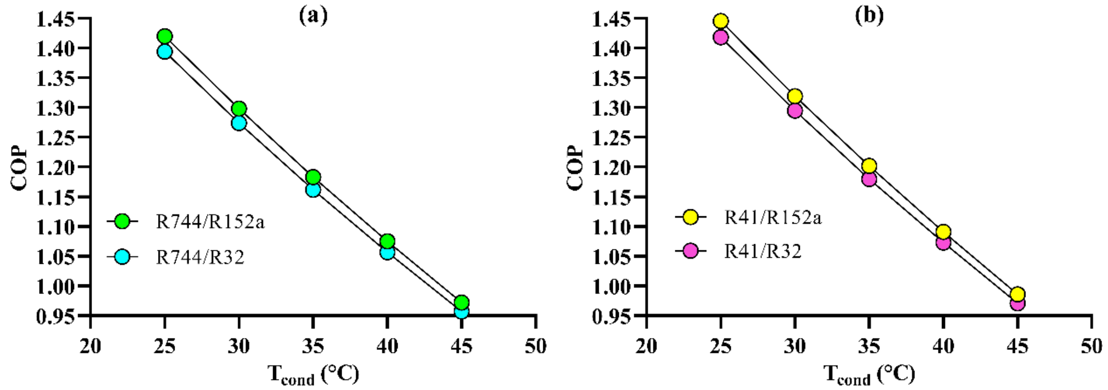


**Figure 6.** Change of COP under various condenser temperatures

Figure 7 shows the relationship between condenser temperature and exergy efficiency. Exergy efficiency decreased as condenser temperature increased from 25 °C to 45 °C for all refrigerant pairs. Similar results indicating that the exergy efficiency of the cascade refrigeration system decreases with increasing condenser temperature have been highlighted in the literature [6]. Exergy efficiency of a R41/R152a pair declined from 0.5298 to 0.3615, corresponding to a 31.8% decrease. Increasing condenser temperature caused exergy efficiency of a R41/R32 to drop from 0.5199 to 0.356, a 31.5% reduction. R744/R32 experienced an exergy efficiency fall by 31.3%, from 0.5111 to 0.3511. Also, exergy efficiency of a R744/R152a refrigerant pair decreased by 31.5%, from 0.5207 to 0.3565. In conclusion, a R41/R152a consistently shows superior exergy efficiency in comparison with other refrigerant groups, especially under lower condenser temperatures.

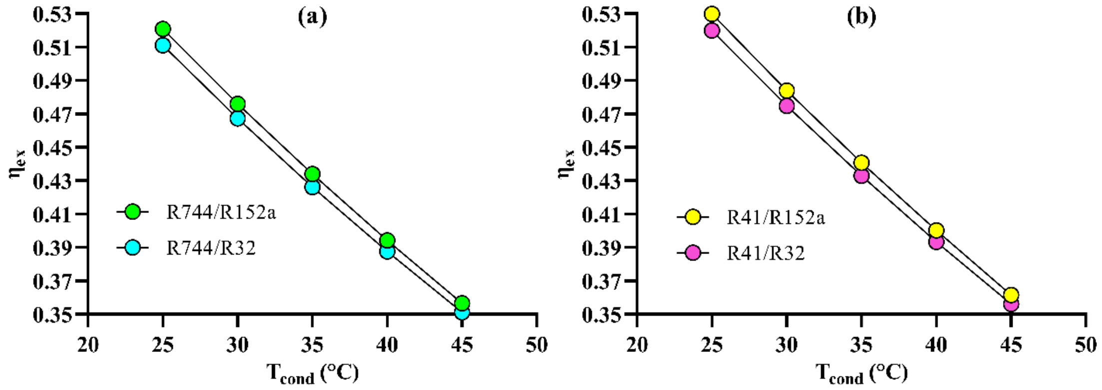


**Figure 7.** Effect of condenser temperature on exergy efficiency

Figure 8 represents the relationship between condenser temperature and total exergy destruction. A rise in condenser temperature from 25 °C to 45 °C led to higher total exergy destruction for all refrigerant groups. Similar findings indicating that the total exergy destruction of the cascade refrigeration system increases with increasing condenser temperature have been presented in the literature [3]. Total exergy destruction of a R41/R152a pair increased from 3.255 to 6.476 kW, a 98.9% rise. A R41/R32 pair experienced a total exergy destruction increase of 95.9%, from 3.386 to 6.633 kW. Increasing condenser temperature resulted with an increase total exergy destruction from 3.376 to 6.62 kW for R744/R152a, meaning a 96% increase. In addition, total exergy destruction of R744/R32 increased by 93.2%, from 3.508 to 6.778 kW. In general, R41/R152a exhibits the least exergy destruction, indicating better exergy performance under varying condenser temperatures.

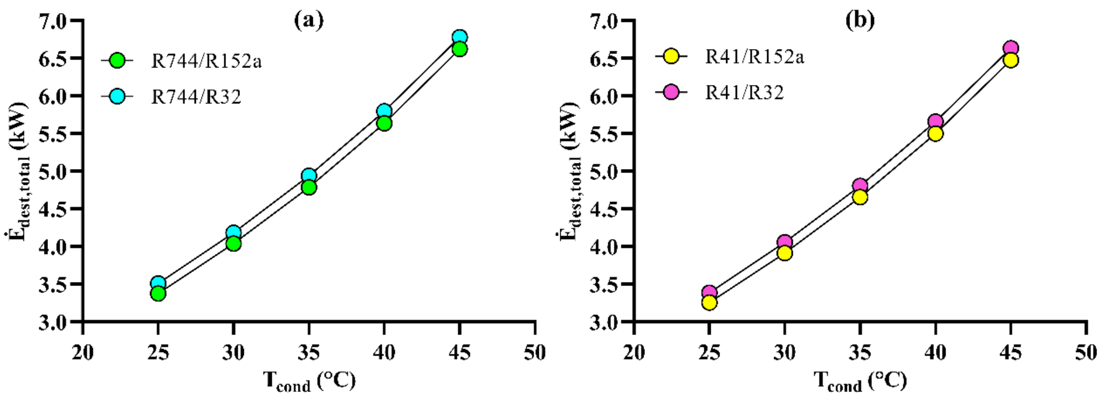


**Figure 8.** Impact of condenser temperature on total exergy destruction

Figure 9 presents the relationship between condenser temperature and total compressor power consumption. Compressor power consumption rose with an increase in condenser temperature from 25 °C to 45 °C. Similar results indicating that the total compressor power consumption of the cascade refrigeration system increases with an increase in condenser temperature have been reported in relevant studies in the literature [15]. Compressor power consumption of a R41/R152a pair increased from 6.922 to 10.14 kW, marking a 46.5% increase. Increasing condenser temperature caused an increase in compressor consumption by 46% for R41/R32 group, from 7.053 to 10.3 kW. For R744/R152a, 46.1% increase in total compressor power was recorded, from 7.043 to 10.29 kW. In addition, R744/R32 showed a 45.5% increase in total compressor consumption, from 7.175 to 10.44 kW. To sum up, R41/R152a shows the lowest compressor power requirement, strengthening its position as the most energy-efficient pair.

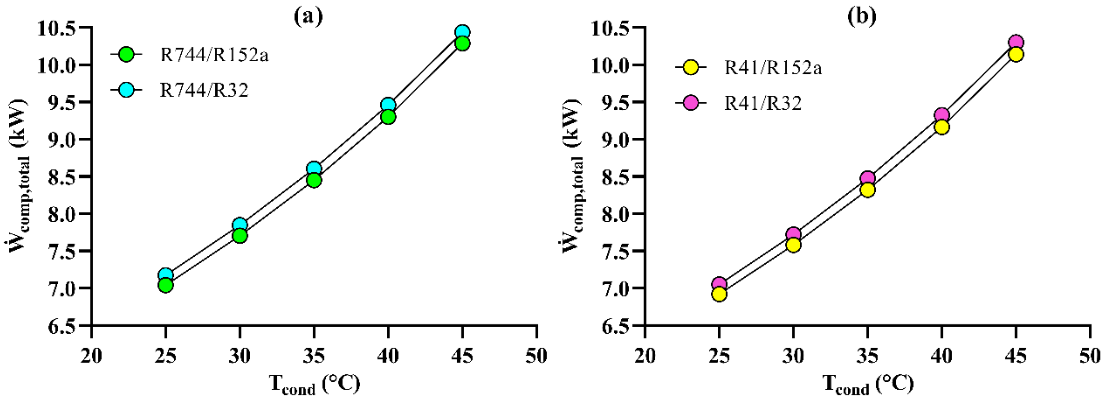


**Figure 9.** Condenser temperature and total compressor consumption relation

Table 5 summarizes the trends obtained from the parametric analysis.

**Table 5.** Effect of change of evaporator and condenser temperatures on thermodynamic parameters

| *Parameter* | *Performance Indicator* | *Effect* |
|---|---|---|
| Evaporator Temperature Increase | COP | Increase |
| | Exergy Efficiency | First increase and then decrease after reaching a peak |
| | Total Exergy Destruction | Decrease |
| | Total Compressor Consumption | Decrease |
| Condenser Temperature Increase | COP | Decrease |
| | Exergy Efficiency | Decrease |
| | Total Exergy Destruction | Increase |
| | Total Compressor Consumption | Increase |

## 3.2. Machine learning results with SVM approach

SVM algorithm was selected for this study due to its well-established ability to perform effectively with limited datasets, its robustness against overfitting, and its capacity to model nonlinear relationships through kernel functions. Given that the available dataset consists of a relatively small number of observations, and that the relationships between system parameters and target outputs such as COP and exergy efficiency are inherently nonlinear, SVM was deemed a suitable and efficient modeling approach. For these reasons, the present study focused on the application and performance evaluation of the SVM method.

To enable prediction using the SVM method, a dataset was constructed. In this dataset, evaporator and condenser temperatures were used as input parameters, while COP and exergy efficiency were selected as the output variables to be predicted. The dataset was generated using the data of the R41/R152a refrigerant pair, which was identified as the most efficient refrigerant combination based on the parametric analysis. During the dataset generation process, the evaporation temperature was varied between –70 °C and –50 °C, and the condenser temperature between 25 °C to 45 °C, both in increments of 2.5 °C. All possible combinations of evaporation and condenser temperatures within these ranges were included in the dataset. For instance, when the evaporator temperature was –70 °C, the condenser temperature was varied across 25, 27.5, 30, 32.5, 35, 37.5, 40, 42.5, and 45 °C. This process was then repeated for evaporator temperatures of –67.5, –65, –62.5, –60, –57.5, –55, –52.5, and –50 °C, with the condenser temperature adjusted accordingly as described. Seventy percent of the dataset was allocated for training, while the remaining thirty percent was used for testing. Each dataset created for the prediction of COP and exergy efficiency consists of 243 data points. The training set contains 168 data points, while the test set includes 75 data points. To ensure the reliability of the predictions, care was taken to maintain a clear distinction between the data used in the training and test sets. The performance of the predictions was evaluated using statistical metrics, specifically the MAE and RMSE, the formulations of which are given below [39]. In these equations, the predicted value is denoted by y, the actual value by x, and the number of samples by n.

$$MAE=\frac{|y_1-x_1|+\ldots+|y_n-x_n|}{n} \tag{9}$$

$$RMSE=\sqrt{\frac{1}{n}\sum_{i=1}^{n}\left(y_i-x_i\right)^2} \tag{10}$$

Figure 10 and Figure 11 present the prediction results for COP and exergy efficiency, covering both the training and test datasets. In Figure 10 and Figure 11, the predictions obtained using the SVM method are represented by light blue circles. The COP and exergy efficiency values obtained from numerical analysis are illustrated by the red y=x line. The proximity of the blue circles to the red y=x line indicates the prediction accuracy of the machine learning method used.

Figure 10 shows the COP prediction results obtained using the SVM method. As observed in Figure 10, the predicted COP values are very close to the actual COP values obtained from numerical analysis, which is evident from the near-perfect alignment of the light blue circles along the diagonal line. The results yielded an MAE of 0.0015 and an RMSE of 0.0033 for the training dataset. For the test set, the MAE and RMSE were 0.0040 and 0.0064, respectively.

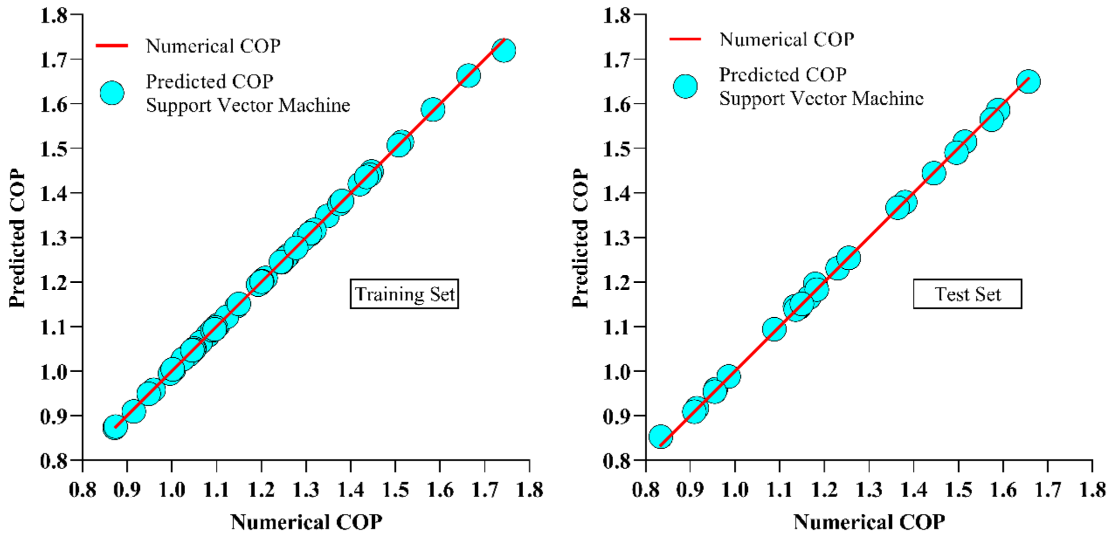


**Figure 10.** COP prediction results

Figure 11 illustrates the exergy efficiency prediction results generated using the SVM algorithm. A close examination of Figure 11 reveals that the predicted exergy efficiency values align remarkably well with the actual values obtained from numerical analysis, as demonstrated by the tight clustering of the light blue circles along the diagonal reference line. For the training dataset, the model achieved a MAE of 0.0003 and an RMSE of 0.0004. In the testing dataset, the corresponding MAE and RMSE values were 0.0009 and 0.0015, respectively.

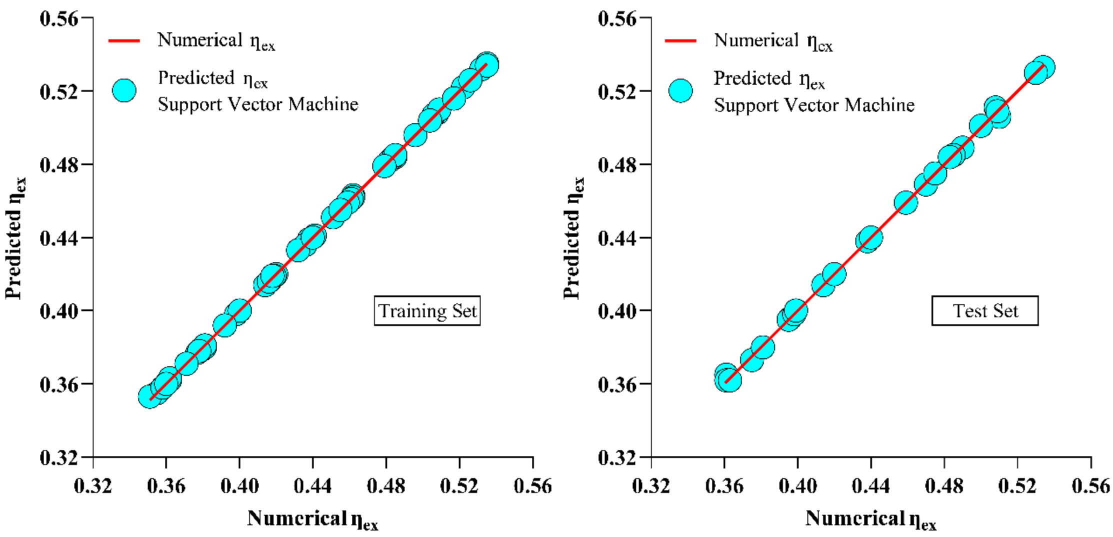


**Figure 11.** Exergy efficiency prediction results

Figure 12 and Figure 13 display the prediction errors of COP and exergy efficiency obtained using the SVM method. In Figure 12 and Figure 13, the error values shown on the y-axis represent the variation between the estimated values and the corresponding numerical data. The x-axis denotes the index of each data point within the complete dataset, which includes both the training and test samples. The prediction errors generated by the SVM model are illustrated by black lines. A value of zero on the y-axis indicates a perfect match between the predicted and numerical values. Significant deviations from zero imply poor prediction accuracy, reflecting a large discrepancy between predicted and actual values, whereas smaller deviations suggest better prediction performance.

An analysis of the COP prediction errors presented in Figure 12 reveals that the maximum error in the training dataset is 0.023. In the test dataset, the biggest COP prediction error was found to be 0.019. The relatively low prediction errors indicate that a successful model for COP prediction has been developed using the SVM method.

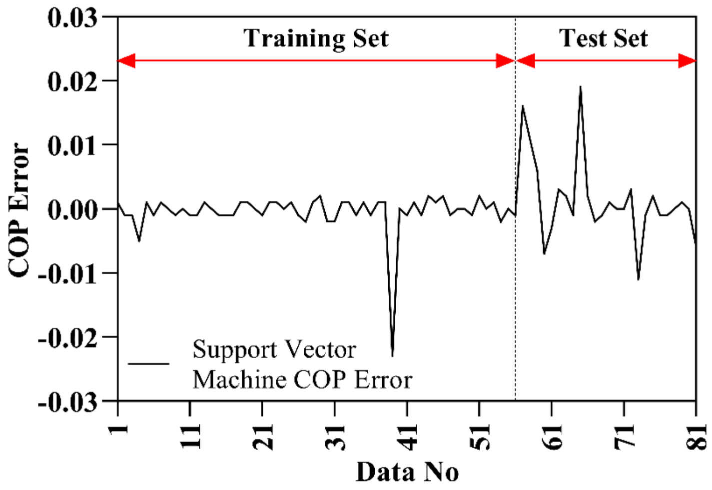


**Figure 12.** COP prediction errors

Upon examining the exergy efficiency prediction errors shown in Figure 13, it is observed that the highest error in the training set is 0.002. For the test set, the maximum exergy efficiency prediction error was 0.004.

The minimal prediction errors suggest that an effective model for exergy efficiency prediction has been established using the SVM method.

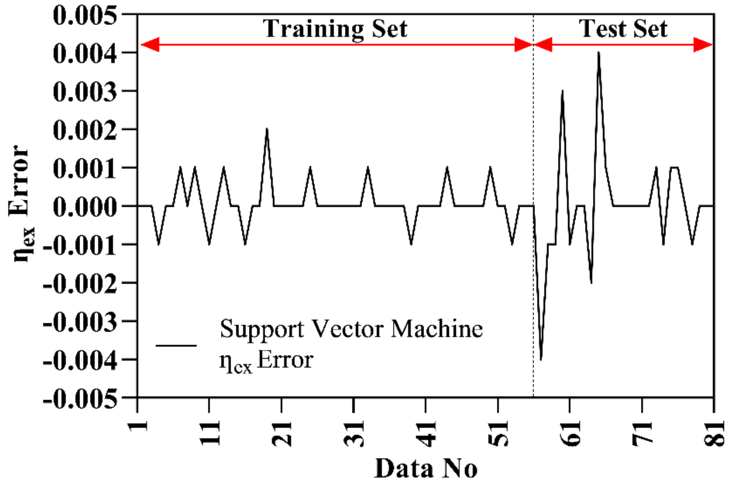


**Figure 13.** Exergy efficiency prediction errors

## 4. Conclusions

In this study, a thermodynamic analysis was conducted for a two-stage cascade refrigeration cycle. The performance of four different refrigerant pairs was evaluated under varying evaporator and condenser temperatures. Through a series of parametric analyses, the most efficient refrigerant pair and the corresponding optimal operating parameters were identified. In the subsequent phase of the study, SVM was applied to the system data to predict the COP and exergy efficiency. The key findings of this work are summarized below:

1. Increasing the evaporator temperature from –70 °C to –50 °C led to an improvement in COP and a rise in exergy efficiency up to a certain point, after which a declining trend was observed. Additionally, both compressor power consumption and exergy destruction decreased with rising evaporator temperature. Conversely, increasing the condenser temperature from 25 °C to 45 °C resulted in reductions in both COP and exergy efficiency, along with increases in exergy destruction and compressor power demand, thus degrading overall system performance.
2. The thermodynamic analysis revealed that the most effective refrigerant pair was R41/R152a. For this combination, the system achieved a maximum COP of 1.421, a peak exergy efficiency of 0.4407, a minimum exergy destruction of 3.971 kW, and a minimum compressor power consumption of 7.039 kW under varying evaporator conditions.
3. Among the predictive models used, the SVM model with a PUK kernel yielded the most accurate estimates. It achieved an MAE of 0.0040 and an RMSE of 0.0064 for COP, and an MAE of 0.0009 and an RMSE of 0.0015 for exergy efficiency in the dataset prepared for testing the model.

The increasing demand for refrigeration systems operating at ultra-low temperatures has motivated the design of a two-stage cascade refrigeration system in this study. The findings are expected to provide valuable insights for researchers and industrial stakeholders involved in low-temperature refrigeration system development. Moreover, the successful performance carried out by the SVM approach in accurately modeling the performance parameters of the cascade system is a notable aspect of the research. This study enhances the existing body of knowledge by providing a comprehensive thermodynamic parametric analysis of a two-stage cascade refrigeration system and developing an accurate predictive model based on the SVM algorithm. The proposed approach offers a robust framework for the optimal design and performance forecasting of ultra-low temperature refrigeration systems. In summary, this research highlights that artificial intelligence techniques are valuable decision-making aids for forecasting, system configuration, and enhancing the performance of cascade refrigeration systems. Future studies are planned to develop an experimental setup to investigate the performance of cascade refrigeration systems capable of operating at ultra-low temperatures.

## 5. Author Contribution Statement

In this study, all processes including the literature review on the analyzed cascade refrigeration system, thermal design, energy and exergy analyses, prediction using SVM, and analysis of the results were carried out by Author 1.

## 6. Ethics Committee Approval and Conflict of Interest Statement

Ethics committee approval was not required for the preparation of this article. The author declares no conflict of interest regarding this study.

## 7. Nomenclature and Subscripts

| | |
|---|---|
| ANN | Artificial Neural Network |
| ASHRAE | American Society of Heating, Refrigerating and Air-Conditioning Engineers |
| COP | Coefficient of Performance |
| CRS | Cascade Refrigeration System |
| EES | Engineering Equation Solver |
| GWP | Global Warming Potential |
| MAE | Mean Absolute Error |
| NBP | Normal Boiling Point |
| ODP | Ozone Depletion Potential |
| RMSE | Root Mean Square Error |
| SVM | Support Vector Machine |
| e | Specific Exergy (kJ/kg) |
| $\dot{E}$ | Flow Exergy (kW) |
| h | Enthalpy (kJ/kg) |
| $\dot{m}$ | Mass Flow Rate (kg/s) |
| $\eta$ | Efficiency |
| $\dot{Q}$ | Heat Transfer Rate (kW) |
| T | Temperature (°C) |
| $\dot{W}$ | Compressor Consumption (kW) |
| $\Delta T$ | Temperature Difference (°C) |
| evap | Evaporator |
| CHX | Cascade Heat Exchanger |
| comp | Compressor |
| cond | Condenser |
| dest | Destruction |
| HTC | High-Temperature Circuit |
| i | Any Point in System |
| LTC | Low-Temperature Circuit |
| 0 | Dead-State |

## 8. Ethical Statement Regarding the Use of Artificial Intelligence

No artificial intelligence-based tools or applications were used in the preparation of this study. The entire content of the study was produced by the author in accordance with scientific research methods and academic ethical principles.

## 9. References

[1] A. Mota-Babiloni *et al.*, “Ultralow-temperature refrigeration systems: Configurations and refrigerants to reduce the environmental impact,” *Int. J. Refrig.*, vol. 111, pp. 147–158, 2020.
[2] C. M. Udroiu, A. Mota-Babiloni, and J. Navarro-Esbri, “Advanced two-stage cascade configurations for energy-efficient -80°C refrigeration,” *Energy Convers. Manag.*, vol. 267, 115907, Sep. 1, 2022.
[3] W. Ye, F. Liu, Y. Yan, and Y. Liu, “Application of response surface methodology and desirability approach to optimize the performance of an ultra-low temperature cascade refrigeration system,” *Appl. Therm. Eng.*, vol. 239, 2024.
[4] S. Khalilzadeh, A. H. Nezhad, and F. Sarhaddi, “Reducing the power consumption of cascade refrigeration cycle by a new integrated system using solar energy,” *Energy Convers. Manag.*, vol. 200, 112083, 2019.
[5] O. Pektezel, M. Das, and H. I. Acar, “Experimental analysis of different refrigerants’ thermal behavior and predicting their performance parameters,” *J. Thermophys. Heat Transf.*, vol. 37, no. 2, pp. 309–319, 2023.
[6] A. Ustaoglu *et al.*, “Performance optimization and parametric evaluation of the cascade vapor compression refrigeration cycle using Taguchi and ANOVA methods,” *Appl. Therm. Eng.*, vol. 180, 2020.
[7] S. Asgari, A. Noorpoor, and F. A. Boyaghchi, “Parametric assessment and multi-objective optimization of an internal auto-cascade refrigeration cycle based on advanced exergy and exergoeconomic concepts,” *Energy*, vol. 125, pp. 576–590, 2017.
[8] R. Llopis *et al.*, “Energy and environmental comparison of two-stage solutions for commercial refrigeration at low temperature: Fluids and systems,” *Appl. Energy*, vol. 138, pp. 133–142, 2015.
[9] A. Mota-Babiloni *et al.*, “Optimisation of high-temperature heat pump cascades with internal heat exchangers using refrigerants with low global warming potential,” *Energy*, vol. 165, pp. 1248–1258, 2018.
[10] W. L. Luyben, “Estimating refrigeration costs at cryogenic temperatures,” *Comput. Chem. Eng.*, vol. 103, pp. 144–150, 2017.
[11] M. W. Faruque *et al.*, “A Comprehensive Thermodynamic Assessment of Cascade Refrigeration System Utilizing Low GWP Hydrocarbon Refrigerants,” *Int. J. Thermofluids*, vol. 15, 2022.
[12] Z. Sun *et al.*, “Comparative analysis of thermodynamic performance of a cascade refrigeration system for refrigerant couples R41/R404A and R23/R404A,” *Appl. Energy*, vol. 184, pp. 19–25, 2016.
[13] W. Ye *et al.*, “Parametric analysis and performance prediction of an ultra-low temperature cascade refrigeration freezer based on an artificial neural network,” *Case Stud. Therm. Eng.*, vol. 55, 2024.
[14] M. Chen *et al.*, “Performance comparison of ultra-low temperature cascade refrigeration cycles using R717/R170, R717/R41 and R717/R1150 to replace R404A/R23,” *Therm. Sci. Eng. Prog.*, vol. 44, 2023.
[15] S. Ji *et al.*, “Energy, exergy, environmental and exergoeconomic (4E) analysis of an ultra-low temperature cascade refrigeration system with environmental-friendly refrigerants,” *Appl. Therm. Eng.*, vol. 248, 2024.
[16] A. K. Vuppaladadiyam *et al.*, “Progress in the development and use of refrigerants and unintended environmental consequences,” *Sci. Total Environ.*, vol. 823, 153670, 2022.
[17] K. Uddin and B. B. Saha, “An overview of environment-friendly refrigerants for domestic air conditioning applications,” *Energies*, vol. 15, no. 21, 8082, 2022.
[18] N. Abas *et al.*, “Natural and synthetic refrigerants, global warming: A review,” *Renew. Sustain. Energy Rev.*, vol. 90, pp. 557–569, 2018.
[19] A. Atmaca *et al.*, “Thermodynamic performance of the transcritical refrigeration cycle with ejector expansion for R744, R170, and R41,” *Isı Bilimi ve Tekniği Dergisi*, vol. 38, no. 2, pp. 111–127, 2018.
[20] A. Usman *et al.*, “Viability of the Proposed Alternative Refrigerants as Future Refrigerants,” *Macromol. Symp.*, vol. 414, no. 1, 2025.
[21] Y. Heredia-Aricapa *et al.*, “Overview of low GWP mixtures for the replacement of HFC refrigerants: R134a, R404A and R410A,” *Int. J. Refrig.*, vol. 111, pp. 113–123, 2020.

[22] A. Mota-Babiloni *et al.*, “Refrigerant R32 as lower GWP working fluid in residential air conditioning systems in Europe and the USA,” *Renew. Sustain. Energy Rev.*, vol. 80, pp. 1031–1042, 2017.
[23] V. H. Panato *et al.*, “Experimental evaluation of R32, R452B and R454B as alternative refrigerants for R410A in a refrigeration system,” *Int. J. Refrig.*, vol. 135, pp. 221–230, 2022.
[24] A. Maiorino *et al.*, “R-152a as an alternative refrigerant to R-134a in domestic refrigerators: An experimental analysis,” *Int. J. Refrig.*, vol. 96, pp. 106–116, 2018.
[25] B. Bolaji, “Experimental study of R152a and R32 to replace R134a in a domestic refrigerator,” *Energy*, vol. 35, no. 9, pp. 3793–3798, 2010.
[26] S. A. Klein, “Engineering Equation Solver (EES),” Academic Professional Version, F-Chart Software: Middleton, 2013.
[27] R. Roy and B. K. Mandal, “Energetic and exergetic performance comparison of cascade refrigeration system using R170-R161 and R41-R404A as refrigerant pairs,” *Heat Mass Transf.*, vol. 55, no. 3, pp. 723–731, 2018.
[28] Z. Sun *et al.*, “Energy and exergy analysis of low GWP refrigerants in cascade refrigeration system,” *Energy*, vol. 170, pp. 1170–1180, 2019.
[29] O. E. Akay and M. Das, “Modeling the total heat transfer coefficient of a nuclear research reactor cooling system by different methods,” *Case Stud. Therm. Eng.*, vol. 25, 100914, 2021.
[30] M. Türk, C. Haydaroglu, and H. Kılıç, “Machine Learning-Based Detection of Non-Technical Losses in Power Distribution Networks,” *Fırat Univ. J. Exp. Comput. Eng.*, vol. 4, no. 1, pp. 192–205, 2025.
[31] A. B. Tatar, “Predicting Three-Dimensional (3D) Printing Product Quality with Machine Learning-Based Regression Methods,” *Fırat Univ. J. Exp. Comput. Eng.*, vol. 4, no. 1, pp. 206–225, 2025.
[32] O. Pektezel and H. I. Acar, “Experimental comparison of R290 and R600a and prediction of performance with machine learning algorithms,” *Sci. Technol. Built Environ.*, vol. 29, no. 5, pp. 508–522, 2023.
[33] S. Salcedo-Sanz *et al.*, “Support vector machines in engineering: an overview,” *Data Min. Knowl. Discov.*, vol. 4, no. 3, pp. 234–267, 2014.
[34] M. E. Cholette *et al.*, “Using support vector machines for the computationally efficient identification of acceptable design parameters in computer-aided engineering applications,” *Expert Syst. Appl.*, vol. 81, pp. 39–52, 2017.
[35] M. Bansal, A. Goyal, and A. Choudhary, “A comparative analysis of K-nearest neighbor, genetic, support vector machine, decision tree, and long short term memory algorithms in machine learning,” *Decis. Anal. J.*, vol. 3, 100071, 2022.
[36] N. Akgün, “Testing The Performance of Random Forest and Support Vector Machine Algorithms for Predicting Cyclist Casualty Severity,” *Fırat Univ. J. Exp. Comput. Eng.*, vol. 2, no. 3, pp. 124–133, 2023.
[37] M. Das, E. Alic, and E. K. Akpinar, “Detailed analysis of mass transfer in solar food dryer with different methods,” *Int. Commun. Heat Mass Transf.*, vol. 128, 105600, 2021.
[38] Y. E. Güzelel *et al.*, “New multiple regression and machine learning models of rotary desiccant wheel for unbalanced flow conditions,” *Int. Commun. Heat Mass Transf.*, vol. 134, 106006, 2022.
[39] O. Pektezel, M. Das, and H. I. Acar, “Experimental exergy analysis of low-GWP R290 refrigerant and derivation of exergetic performance equations with regression algorithms,” *Int. J. Exergy*, vol. 40, no. 4, pp. 467–482, 2023.